

Hydrogen-Bond Assisted, Concentration Dependent Molecular Dimerization of Ferrocenyl-Hydantoins

Annalisa Bisello,[†] Roberta Cardena,[†] Serena Rossi,[†] Marco Crisma,[‡] Fernando Formaggio[†] and Saverio Santi^{*,†}

[†]Department of Chemical Sciences, University of Padova, via Marzolo 1, 35131 Padova, Italy

[‡]Institute of Biomolecular Chemistry, Padova Unit, CNR, via Marzolo 1, 35131 Padova, Italy

Supporting Information Placeholder

ABSTRACT: The synthesis and characterization of the ferrocenyl methylhydantoin (5-ferrocenyl-5-methylimidazolidine-2,4-dione), efficiently prepared through Bucherer–Bergs reaction, and its derivatives carrying tert-butoxycarbonyl (Boc) protecting groups, namely 1,3-di(tert-butoxycarbonyl)-5-ferrocenyl-5-methylimidazolidine-2,4-dione and 1-(tert-butoxycarbonyl)-5-ferrocenyl-5-methylimidazolidine-2,4-dione, are reported. X-Ray diffraction and ESI-Mass spectrometry analyses of the ferrocenyl methylhydantoin revealed the presence of C=O⋯H–N intermolecularly hydrogen bonded dimers. The mono-Boc derivative displayed to form a hydrogen-bonded dimer in solution, as confirmed by ¹H-NMR, FT-IR and cyclic voltammetry experiments at different concentrations in CDCl₃ or CHCl₃.

INTRODUCTION

Hydantoin (imidazolidine-2,4-dione) is an important cyclic imide used in medicinal chemistry. Due to its broad spectrum of biological activities it is a leading compound for the synthesis of drugs with anticonvulsant, antiparasite, and anticancer activities.¹ Indeed, hydantoins derivatives can be found in a wide array of drugs and biologically active compounds² and are also important intermediates in the synthesis of α -amino acids.³

Hydantoin, possessing two N-H donors and two C=O acceptors, appears a structurally attractive species for the study of noncovalent molecular interactions, such as intermolecular hydrogen bonding.⁴ Moreover, the N-H hydrogens are crucial for interactions with solvents. Therefore, the characterization of these interactions is of fundamental interest for the in depth understanding of structural and mechanistic aspects. In fact, multiple hydrogen bonds are useful building blocks for assembling complex systems because they can set molecules in particular geometries, by virtue of their directionality.

In addition, it was previously shown that the incorporation of a ferrocenyl unit into hydantoin rings⁵ or other organic moieties⁶ leads to ferrocenyl compounds showing a strong cytotoxic effect. Interestingly, the introduction of the ferrocenyl moiety into the side chain of chloroquine yielded ferroquine, a well-known drug with higher antimalarial activity compared to chloroquine and other organometallic compounds.⁷

Besides, ferrocenyl derivatives were intensely studied because of their potential applications in many fields such as optoelectronic materials, catalysts and biochemical redox or photonic devices.⁸ They present a remarkably flexible conformation, caused by the free rotation of the cyclopentadi-

enyl moieties. Also, the redox behavior between the neutral Fe(II) state and the cationic Fe(III) state, involving fast and reversible electron transfer (ET), is an important property that is very well described in the literature.⁹

Furthermore, ferrocene and its derivatives are the most commonly used mediators in amperometric biosensors.¹⁰ For instance, ferrocenyl-urea¹¹ and ferrocenyl-ureidopyrimidine¹² derivatives were used as receptors of host molecules forming multiple hydrogen-bonding arrays. The introduction of the redox-active ferrocene moiety into these systems makes it feasible to follow or even modify interactions by electrochemical methods.

In the last few decades, ferrocenyl amino acids¹³ and peptides¹⁴ received remarkable attention because they reflect properties of both ferrocene and biological moieties. Ferrocene was exploited as organometallic scaffold for the assembly of foldamers via intramolecular H-bonding and as a redox probe in the study of ET through peptides and other biomolecules.¹⁵ For example, self-assembled monolayers (SAMs) Fc-terminated α -helical peptides served as suitable model systems for studying the ET through helical peptides.¹⁶

Recently, we reported the synthesis and the characterization of new series of 3₁₀-helical peptides of different lengths and rigidity. They are based on the strongly helix inducer α -aminoisobutyric acid (Aib) and contain one terminal ferrocenyl unit,^{14e} namely Z-(Aib)_n-NH-Fc (Z = benzyloxycarbonyl, n = 1-5) and Fc-CO-(Aib)_n-OMe (OMe, methoxy, n = 1-5), or two,^{14f} Fc-CO-(Aib)_n-NH-Fc (n = 1-5). In the two series of monometallic ferrocenyl-peptides the position of the ferrocenyl groups, at the positive or negative end of the helix macrodipole, had a remarkable effect on the trends of the oxidation potentials. In the bimetallic ferrocenyl pep-

tides, the intrinsic redox asymmetry of the C-terminal and N-terminal ferrocenyl groups allowed to generate, selectively, the cationic and dicationic derivatives. The end-to-end effects of the charge holes generated by single and double oxidations were studied by means of electrochemical and spectroelectrochemical techniques. In particular, in the pentapeptide, charge was transferred through an intramolecular iron–iron separation of 14 Å. Since no intervalence transition bands were observed for the end-capped bis(ferrocenyl) peptides, the end-to-end effects of the charge holes generated by single oxidation could be explained by inductive and/or electrostatic interactions transmitted through the intramolecularly H-bonded networks.

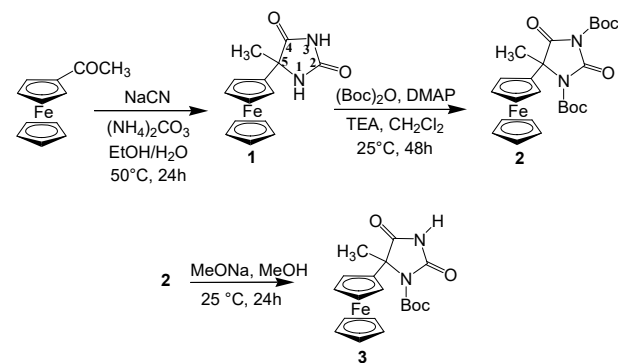
Besides covalently linked structures, it is also imaginable to design intermolecularly H-bonded molecules connecting redox centers. However, in spite of the exceptional information that these systems would provide to ET processes in DNA and other biological systems, it is surprising that only a few examples have been reported so far.¹⁷

Herein we present the synthesis and the characterization of ferrocenylmethylhydantoin (5-ferrocenyl-5-methylimidazolidine-2,4-dione) (1) and its Boc (tert-butoxycarbonyl) derivatives 1,3-diBoc-5-ferrocenyl-5-methylimidazolidine-2,4-dione (2), and 1-Boc-5-ferrocenyl-5-methylimidazolidine-2,4-dione (3). The aim was to explore the possible formation of H-bond-assisted molecular dimers, through C=O···H–N interactions, by exploiting the efficient ferrocenyl electrochemical probe.

RESULTS AND DISCUSSION

Synthesis. The synthesis of 5-ferrocenyl-5-methylimidazolidine-2,4-dione (1) was performed through the Bucherer–Bergs method¹⁸ (Scheme 1).

Scheme 1. Syntheses of Compounds 1–3.



Acetylferrocene was treated with sodium cyanide in the presence of ammonium carbonate at 50 °C for 24 hours to afford 1 in good yield. The treatment of 1 with bis(*tert*-butyl)dicarbonate (Boc₂O) in CH₂Cl₂, in the presence of 4-(dimethylamino)pyridine (DMAP) and triethylamine (TEA), furnished the corresponding di-Boc derivative (2). Then, the mono-Boc derivative (3) was obtained by treating 2 with NaOMe in methanol.

Molecular structures. The molecular structures of compounds 1 and 2, as determined by single crystal X-ray diffraction analysis, are illustrated in Figure 1 (panels A and B, respectively). Both compounds were synthesized as race-

mates. Compound 1 crystallized in a centrosymmetric space group, in which both enantiomers co-exist, and the isomer of *R* configuration at C1 (shown in Figure 1, top) was arbitrarily selected as the asymmetric unit.

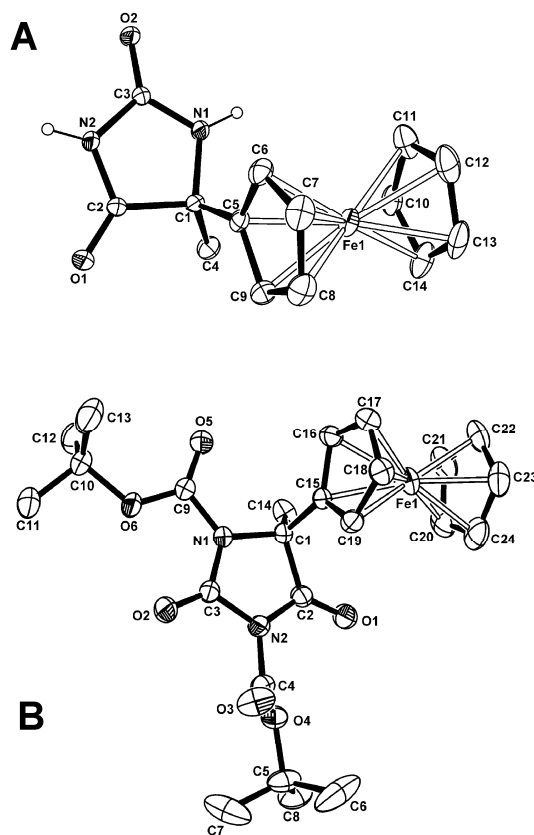


Figure 1. X-Ray diffraction structures of: (A) 5-ferrocenyl-5-methylimidazolidine-2,4-dione (1), and (B) its 1,3-di-Boc derivative (2) with atom numbering. In both structures, only the major occupancy site for the distal cyclopentadienyl ring is shown. Anisotropic displacement parameters for the non-hydrogen atoms are drawn at the 30% probability level. Hydrogen atoms are omitted for clarity, except those on nitrogens in 1.

Conversely, compound 2 crystallized in the acentric P2₁2₁2₁ space group (in which molecules of only one handedness are present), but the crystal turned out to be twinned by inversion. The fractions of the two twin components are equal within experimental error (see Experimental Section for details). The atomic coordinates of 2 and the related torsion angles discussed in the following refer to the (*S*)-enantiomer depicted in the bottom part of Figure 1. In both structures, the distal cyclopentadienyl (Cp) ring showed rotational disorder and was refined on two sets of positions. In 1, the angles between the normal to the proximal Cp ring and those of the major and minor occupancy sites of the distal Cp are 2.7(4)° and 4.1(3)°, respectively. The corresponding angles found for 2 are 2.5(3)° and 4.0(6)°. The values of the average H–C – C–H inter-ring angles of twist are -13.1° and 3.2°, respectively, for the major and minor occupancy sites of the distal Cp for compound 1, while -9.8° and 14.7°, respectively, for 2. Overall, these ferrocene conformations can be described as nearly eclipsed.

The Fe–C bond lengths range from 1.951(14) to 2.148(12) Å in compound **1**, while from 1.991(12) to 2.156(23) Å in compound **2**. In both cases, the extreme values involve atoms of the disordered, distal Cp rings. Fe–C bond length distributions are much narrower for the proximal Cp rings, in the range 2.0313(15) – 2.042(2) Å for **1**, and 2.026(3) – 2.057(3) Å for **2**.

In both structures, the hydantoin and ferrocenyl moieties are nearly perpendicular to each other. The angles between normals to the average plane of the hydantoin and of the proximal Cp ring are 81.30(7)° in **1** and 79.40(10)° in **2**. However, differences are observed for the torsion angles about the C–C bond connecting the aforementioned groups. Specifically, for **1**, the values of the N1–C1–C5–C6 and N1–C1–C5–C9 torsion angles are 26.0(2)° and -161.71(15)°, respectively, whereas for **2** the values of the corresponding N1–C1–C15–C16 and N1–C1–C15–C19 torsion angles are -89.0(3)° and 82.9(3)°, respectively.

Interestingly, in **2**, the urethane carbonyl oxygens O3 and O5 are positioned differently with respect to the hydantoin ring. Specifically, O5 is coplanar [within 0.044(3) Å] to the average plane of the hydantoin, whereas O3 is displaced by 1.073(3) Å. This latter finding is related to the values adopted by the torsion angles C3–N2–C4–O3 [-53.3(5)°] and C2–N2–C4–O3 [122.5(4)°]. Values close to 0° / 180° or 180° / 0° for this pair of torsion angles are strongly disallowed, as they would bring the distance of O3 from either O1 or O2 as short as 2.60 Å. Conversely, the C3–N1–C9–O5 torsion angle is *trans* [172.2(3)°]. The twist about the urethane N2–C4 bond is expected to affect the electron delocalization of the π -system. Indeed, the N2–C4 bond, 1.434(4) Å, is 0.03 Å longer than the corresponding N1–C9 bond [1.405(4) Å] of the planar urethane moiety on N1. Similar findings were previously reported for a fully Boc-protected piperidine-spiro-hydantoin.¹⁹ Overall, these geometrical features suggest that the Boc group on N2 might be more labile than that on N1, thus accounting for its regioselective removal observed in the reaction of **2** with sodium methoxide in methanol, which afforded the 1-Boc derivative **3** in excellent yield.

In the packing mode of **1** (Figure 2), the N2–H2 group is intermolecularly H-bonded to the (-x, -y, 2-z) symmetry

equivalent of the O2 carbonyl oxygen, thus generating doubly H-bonded centrosymmetric dimers. It is worth recalling that hydantoins can form six different types of doubly H-bonded dimers.²⁰ The type observed for **1** (in which the N–H donor and the C=O acceptor are at ring positions 3 and 2, respectively) is shared by only 8 out of 83 entries of 5,5-disubstituted hydantoins, the structures of which are available in the Cambridge Structural Database (version 5.37, Nov. 2015).²¹ A second type of intermolecular H-bond is observed between the N1–H1 group and a (1/2-x, -1/2+y, z) symmetry equivalent of O1, connecting molecules in a zig-zag motif along the b direction. The N2–H2...O2 hydrogen bond, characterized by N...O and H...O separations of 2.7808(17) and 1.94 Å, respectively, appears to be stronger than the N1–H1...O1 hydrogen bond, for which the N...O and H...O separations are 2.8640(17) and 2.04 Å, respectively.

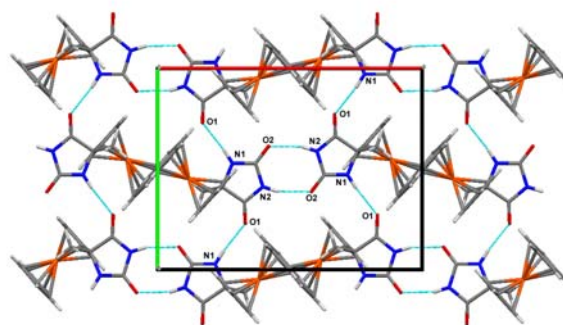


Figure 2. Packing mode of 5-ferrocenyl-5-methyl-imidazolidine-2,4-dione (**1**) as viewed down the *c* axis. Only the major occupancy site for the distal cyclopentadienyl ring is shown. Intermolecular hydrogen bonds are indicated by dashed lines.

The di-Boc derivative **2** lacks any N–H hydrogen-bonding potential donor. Its packing mode is achieved through intermolecular van der Waals interactions and C–H...O contacts. Among the latter, the shortest (H...O separations \leq 2.70 Å) involve H-atoms on C11 and C22, respectively, and the O2 and O3 carbonyl oxygens, respectively, of symmetry-related molecules (the C–H groups belonging to the

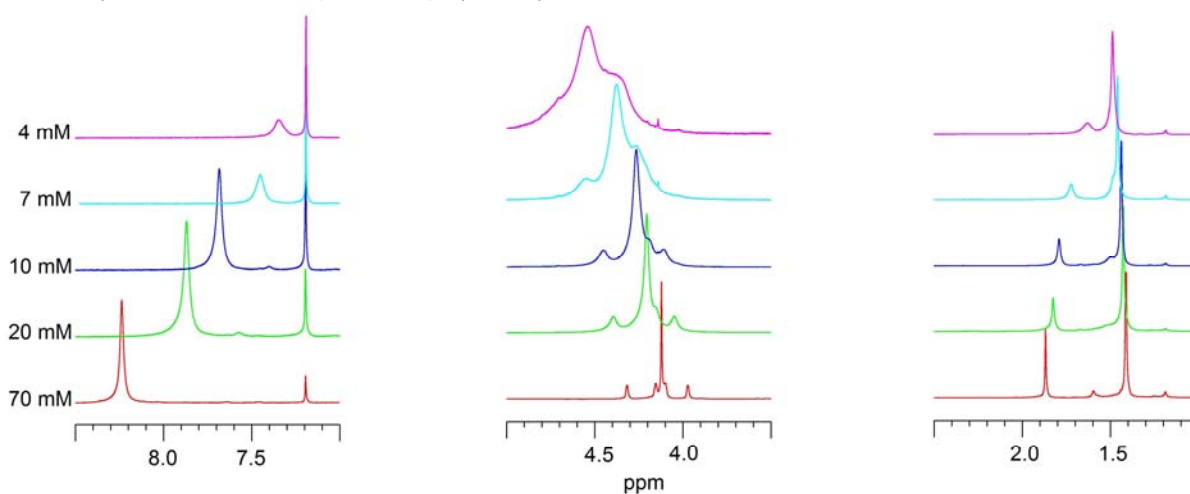
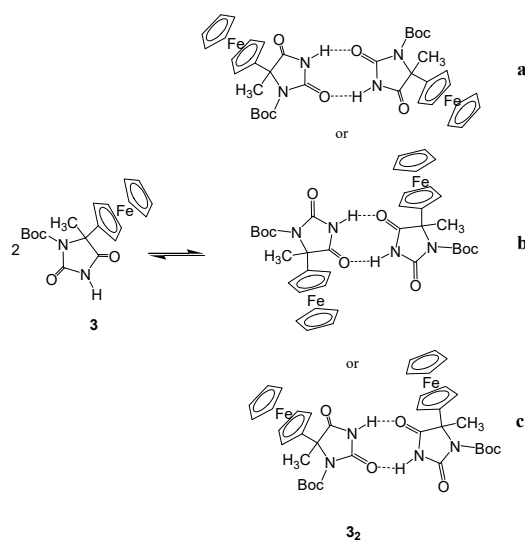


Figure 3. ¹H NMR spectrum (400.13 MHz) of **3** in CDCl₃ at different concentrations.

minor occupancy sites of the distal Cp have been excluded from this analysis).

NMR spectroscopy. Compound **3** undergoes H-bond assisted dimerization (Scheme 2), as suggested by $^1\text{H-NMR}$ (Scheme 2), as suggested by $^1\text{H-NMR}$ (cancellare) experiments in CDCl_3 at different concentrations.²² Upon dilution from 70 mM to 4 mM solutions, the N-H signal of **3** shifted upfield from 8.4 ppm to 7.3 ppm (Figure 3), supporting the role of N-H in forming intermolecular H-bonds at high concentrations. At concentrations lower than 70 mM the ferrocenyl and methyl signals broadened and shifted downfield and upfield, respectively, whilst the Boc signal did not exhibited significant shifts or broadening. On the contrary, the spectrum of **3** in acetone- d_6 solution did not show the H-bonded N-H shift because of the high polarity of this solvent that disrupts the hydrogen bonding interactions (see Experimental Section). These evidences strongly support the prevalence of dimers **3₂** at high concentration.

Scheme 2. Dimerization of **3**.



Among the three different types of doubly H-bonded dimers which **3** can form (Scheme 2) the type **c**, containing nonequivalent N-H, Fc, methyl and Boc groups, can be excluded on the basis of the presence of single signals for each type of hydrogen in the $^1\text{H-NMR}$ spectra of Figure 3.

IR spectroscopy. The dimerization of **3** in CDCl_3 was corroborated also by FT-IR measurements at different concentrations (Figure 4).

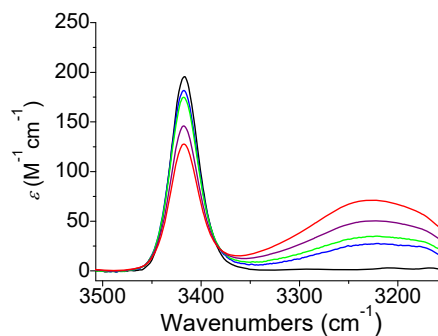


Figure 4 FT-IR absorption spectra in the N-H stretching region in CDCl_3 solution 1 mM (black line), 10 mM (blue line), 20 mM (green line), 40 mM (purple line) and 70 mM (red line) for **3**. The absorbance was corrected for peptide concentration and optical path.

The N-H stretching region allowed us to assess if the N-H groups are involved in $\text{C=O}\cdots\text{H-N}$ H-bonds. Absorptions at $3400\text{--}3450\text{ cm}^{-1}$ are usually associated with free N-H groups, while bands at $3320\text{--}3340\text{ cm}^{-1}$ are related to H-bonded N-H groups.²³ The FT-IR spectra of **3** in CDCl_3 solution show a band centered at 3410 cm^{-1} (free N-H) and, by increasing the concentration from 10 to 70 mM, a broad band at about 3220 cm^{-1} , not observed at concentration of 1 mM. This unusually high-energy absorption can be safely attributed to the formation of strong intermolecular H-bonds at high concentrations. Again, this behavior is in agreement with the formation of H-bonded dimers.

Mass spectrometry. ESI mass spectrometry, an effective tool for investigating the formation of H-bonded species, further confirmed the formation of the H-bonded adduct. Besides the molecular ion peak (M^+) assigned to the monomer, the ESI spectrum of **3** revealed a small peak corresponding to the dimer ($M_2\text{Na}^+$) (see Supporting Information). Contrary to **3**, compound **1** is poorly soluble in halogenated solvents, thus preventing us from investigating its self-association properties by NMR and IR experiments. However, the occurrence of an intense peak assigned to the dimer ($M_2\text{H}^+$) in the ESI spectrum of **1** (see Supporting Information) strongly support the view that even in the gas phase this compound does give rise to a H-bonded complex,²⁴ in all probability similar to that observed in the crystal state.

Electrochemistry. Cyclic voltammograms (CVs) at different concentrations of **3** were obtained under argon in $\text{CHCl}_3/0.1\text{ M } n\text{Bu}_4\text{NB}(\text{C}_6\text{F}_5)_4$ (Figure 5).

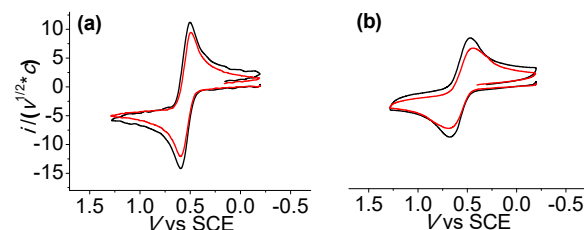


Figure 5. CVs in $\text{CHCl}_3 / 0.1\text{ M } n\text{Bu}_4\text{NB}(\text{C}_6\text{F}_5)_4$ of **3**, $C = 3\text{ mM}$ (black line) and 10 mM (red line), at gold disk working electrode ($d = 125\text{ }\mu\text{m}$). Scan rate ν (a) 0.5 V s^{-1} , (b) 100 V s^{-1} . The current was correct-

ed for the concentration of **3** and the square root of the potential scan rate v .

The compound exhibited one oxidation wave, chemically and electrochemically reversible ($E_{1/2} = 0.54$ V, $i_a/i_p \approx 1$, $E_p - E_{p/2} = 69$ mV at 0.5 Vs^{-1}) as predictable for a Fc/Fc^+ redox couple. The value of $i_{max}/v^{1/2}C$ decreased by increasing the concentration from 3 to 10 mM (Figure 5), an effect observed for the potential scan rates in the range of 0.2–100 Vs^{-1} (Figure 6a).

The two data sets nicely merged when plotted vs $\log v \times C$ (Figure 6b), indicating concentration dependence of the forwards and back reactions of equilibrium reported in Scheme 2, being second and first order, respectively. The sigmoidal fitting of the overall dataset (Figure 6b) indicates that $i_{max}/v^{1/2}C$ tends to constant values for $\log v \times C$ tending to 0 and ∞ .

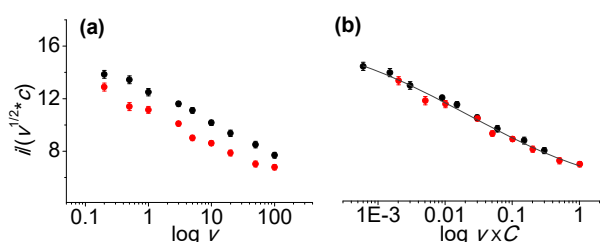


Figure 6. Concentration dependence, $C = 3$ mM (black) and 10 mM (red) **3**, (a) vs $\log v$, (b) vs $\log \log v \times C$. Sigmoidal fitting (dark gray line).

We ascribe this current drop to a difference in the diffusion coefficients of the monomeric and dimeric species, considering that the relative diffusion coefficients depend on their molecular size according to the Stokes-Einstein equation ($D \propto 1/r$).²⁵ Lower values of D and i_{max} are expected for **3₂**.

In fact, for a Nernstian (reversible) ET process, the value of i_{max} of a CV experiment is given by equation 1:²⁶

$$i_{max} = (2.69 \times 10^5) n^{3/2} CAD^{1/2} v^{1/2} \quad (1)$$

where A is the area of the electrode, D and C are diffusion coefficient and the bulk concentration of the electroactive species, respectively, and n is the number of electrons exchanged. Considering that $C_m/C_d = 2$ and $n_m = 1$ and $n_d = 2$ (the subscripts m and d stand for monomer and dimer, respectively) as **3₂** contains two noninteracting ferrocenyl groups (no intervalence transition absorptions were observed in the near-IR region), the square root of the diffusion coefficient ratio (equation 2) results:

$$\left(\frac{D_m}{D_d}\right)^{1/2} = 1.4 \times \frac{\left(i_{max}/v^{1/2}C\right)_{v \rightarrow 0}}{\left(i_{max}/v^{1/2}C\right)_{v \rightarrow \infty}} \quad (2)$$

Since $(i_{max}/v^{1/2}C)_{v \rightarrow 0} \approx 2 (i_{max}/v^{1/2}C)_{v \rightarrow \infty}$ as experimentally observed (Figure 6), it results that $D_m \approx 8D_d$.

The concentration dependence of the current intensity of **3** was also evidenced by differential pulse voltammetry (DPV) experiments (Figure 7). The DPV at 3 mM of **3** and scan rate of 0.5 Vs^{-1} displayed a single and narrow peak at 0.52 V vs SCE.

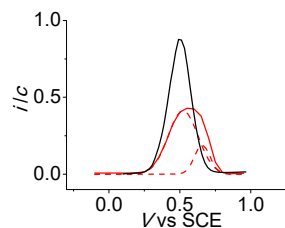
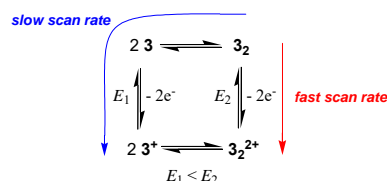


Figure 7. DPVs of **3** in $CHCl_3 / 0.1$ M $nBu_4NB(C_6F_5)_4$, $C = 3$ mM (black line) and 10 mM (red line), at gold disk working electrode ($d = 0.5$ mm). Modulation amplitude of 200 mV; modulation time of 0.05 s; interval time (Δt) of 0.1 s, different step potential (E_{step}) of 0.05 V. Scan rate, $v = E_{step} / \Delta t$, 0.5 Vs^{-1} . The current was corrected for the concentration of **3**. Gaussian deconvolution (red dashed line) of DPVs at 10 mM. The current was corrected for the concentration of **3**.

By increasing the concentration to 10 mM, a broad and less intense peak appeared. Its Gaussian deconvolution displayed the presence of two peaks at 0.52 and 0.66 V vs SCE.

According to NMR and IR results, we attribute the observed concentration effect and the appearance of the new peak at 0.66 V in DPV experiments to the formation of the dimer **3₂** (Scheme 2) which is indeed oxidized at higher potential with respect to monomer **3**.



Scheme 3. Proposed oxidation mechanism.

In particular, the oxidation of the dimer at more positive potential represents a crucial point for the assessment of the redox behavior and justifies the decrease of $i_{max}/v^{1/2}C$ displayed in Figure 6 and 7. In fact, as the oxidation of **3** firstly occurs, at adequately slow scan rate the equilibrium process is dragged to the monomer (Scheme 3). Conversely, if the scan rate is sufficiently fast the dissociation of the dimer has no significant effect, then the oxidation of the dimer **3₂** can occur and the value of $i_{max}/v^{1/2}C$ decreases according to the lower value of its diffusion coefficient ($D_d < D_m$).

CONCLUSIONS

We have successfully synthesized the ferrocenyl methylhydantoin (**1**) and its derivatives carrying one (**3**) or two (**2**) Boc protecting groups at the ring nitrogen atoms. Their characterization was achieved by combining structural analysis together with spectroscopic and electrochemical techniques.

The single crystal X-ray analysis of **1** and **2** showed that the hydantoin and ferrocenyl moieties are nearly perpendicular to each other. Interestingly, in the packing mode of **1** doubly H-bonded centrosymmetric dimers are generated through $C=O \cdots H-N$ intermolecular interactions.

The formation of H-bonded dimers was observed also for compound **3**, in $CDCl_3$ solution. By increasing the concentration of **3** the proton N-H resonance moved downfield in

the ^1H -NMR spectrum, whereas a high-energy absorption band appeared in the NH stretching region of the FT-IR spectrum.

Finally, the H-bond-assisted molecular dimerization was highlighted exploiting the presence of the efficient ferrocenyl electrochemical probe. DPV experiment showed that the dimer **3**₂ is oxidized at higher potential with respect to monomer **3**. The CV oxidation wave of **3** appeared concentration and time dependent. The current drop of the oxidation wave is due to a difference in the diffusion coefficients of the monomeric and dimeric species, being $D_m > D_d$ as the relative diffusion coefficients depend on the molecular size. Since the oxidation of **3** occurs at lower potential, at low scan rates the dimerization equilibrium process is drawn back to the monomer. If the scan is sufficiently fast the dimer dissociation does not occur, then the oxidation of **3**₂ takes place and the current intensity decreases. It is worth noting that the electrochemical analysis allowed detecting the formation of the dimer even if present in a small amount and at relative low concentration as shown by the IR spectrum of **3** at 10 mM.

The multitechnique approach exploited in this study was instrumental in unraveling the $\text{C}=\text{O}\cdots\text{H}-\text{N}$ H-bond-assisted molecular dimerization of **1** and **3**.

EXPERIMENTAL SECTION

General methods. All reactions and complex manipulations were performed in oxygen and moisture-free atmosphere utilizing standard Schlenk techniques. Solvents were dried by reflux over the appropriate drying agent and distilled under stream of Argon. Acetylferrocene, ammonium carbonate, sodium cyanide, di-*tert*-butyldicarbonate, triethylamine, 4-(dimethylamino)pyridine, sodium methoxide solution and anhydrous methanol were Sigma Aldrich products. Microanalyses were performed at the Dipartimento di Scienze Chimiche, Università di Padova. HRMS spectra were obtained using an ESI-TOF Mariner 5220 (Applied Biosystem) mass spectrometer with direct injection of the sample and collecting data in the positive mode. ^1H and ^{13}C NMR spectra were obtained on a Bruker Avance III HD spectrometer operating at 400.13 and 100.61 MHz, respectively ($T = 298\text{ K}$). The assignments of the proton resonances were performed by standard chemical shift correlation and 2D (NOESY and COSY) experiments. The ^{13}C resonances were attributed through 2D-heterocorrelated experiments (HMQC²⁷ for the H-bonded carbon atoms, HMBC²⁷ for the quaternary ones). CV experiments were performed in an air-tight three electrode cell connected to a vacuum/argon line. The reference electrode was a SCE (Tacussel ECS C10) separated from the solution by a bridge compartment filled with the same solvent/supporting electrolyte solution used in the cell. The counter electrode was a platinum spiral with *ca.* 1 cm² apparent surface area. The working electrodes were disks obtained from cross section of gold wires of different diameters (0.5 and 0.125 mm) sealed in glass. Between successive CV scans the working electrodes were polished on alumina according to standard procedures and sonicated before use. An EG&G PAR-175 signal generator was used. The currents and potentials were recorded on a Lecroy 9310L oscilloscope. The potentiostat was home-built with positive feedback loop for compensation of the ohmic drop.²⁸ Autolab PGSTAT 100 potentiostat/galvanostat (EcoChemie, The Netherlands) run by a PC with GPES software was used for the DPV experiments. IR spectra were recorded with Nicolet Nexus 670 FTIR spectrophotometer.

Preparation of 5-ferrocenyl-5-methylimidazolidine-2,4-dione (1). A suspension of acetylferrocene (6.7 g, 29 mmol) in ethanol (25 mL) was treated with a solution of ammonium carbonate (6.7 g, 70 mmol) in water (18 mL). Then at 25 °C a solution of sodium cyanide (1.4 g 29 mmol) in water (8 mL) was added dropwise to the stirred suspension prepared previously. The resulting orange mixture was warmed at 50 °C for 24 hours and filtered. The residue was washed with water (200 mL) and diethylether (300 mL) and evaporated to dryness, yielding **1** as

an orange solid (4.2 g, 49 %). Anal. Calcd for $\text{C}_{14}\text{H}_{14}\text{FeN}_2\text{O}_2$: C, 56.40; H, 4.73. Found: C, 56.38; H, 4.74. HRMS (ESI+): m/z Calcd for $\text{C}_{14}\text{H}_{14}\text{FeN}_2\text{O}_2$ (M+): 298.0405. Found: 298.0530. ^1H NMR (acetone-*d*₆): δ 1.63 (s, 3H, CH₃), 4.21-4.18 (m, 7H, C₅H₅, C₅H₄), 4.25 (m, 1H, C₅H₄), 4.29 (m, 1H, C₅H₄), 7.28 (s, 1H, NH), 9.50 (s, 1H, NH). ^{13}C NMR (acetone-*d*₆): δ 26.75 (CH₃), 62.71 (C5), 66.28 (C₅H₄), 66.85 (C₅H₄), 68.96 (C₅H₄), 69.66 (C₅H₅), 91.34 (C₅H₄, Ci), 156.63 (CO), 176.73 (CO).

Preparation of 1,3-di(*tert*-butoxycarbonyl)-5-ferrocenyl-5-methylimidazolidine-2,4-dione (2). Bis(*tert*-butyl)dicarbonate (1.1 g, 5 mmol), 4-(dimethylamino)pyridine (4 mg, 0.04 mmol), triethylamine (145 μL , 1 mmol) were added to a stirred suspension of **1** (300 mg, 1 mmol) in dichloromethane (4mL) under argon. The solution changed immediately the color from orange to red. The resulting mixture was stirred at room temperature for 48 h. Elimination of the solvent in vacuo and purification by column chromatography (silica gel, pentane/ethyl acetate) afforded 440 mg (88%) of orange product. Anal. Calcd for $\text{C}_{24}\text{H}_{30}\text{FeN}_2\text{O}_6$: C, 57.84; H, 6.07. Found: C, 57.86; H, 6.08. HRMS (ESI+): m/z Calcd for $\text{C}_{24}\text{H}_{30}\text{FeN}_2\text{O}_6$ (M+): 498.1453. Found: 498.1502. ^1H NMR (acetone-*d*₆): δ 1.48 (s, 9H, COOC(CH₃)₃), 1.60 (s, 9H, COOC(CH₃)₃) 1.94 (s, 3H, CH₃) 4.12 (m, 1H, C₅H₄), 4.19 (s, 5H, Cp), 4.22 (m, 1H, C₅H₄), 4.28 (m, 1H, C₅H₄), 4.38 (m, 1H, C₅H₄). ^{13}C NMR (acetone-*d*₆): δ 24.51 (CH₃), 27.96 (COOC(CH₃)₃), 28.17 (COOC(CH₃)₃), 66.15 (C5), 67.05 (C₅H₄), 68.12 (C₅H₄), 68.59 (C₅H₄), 69.11 (C₅H₄), 70.20 (C₅H₅), 84.52 (COOC(CH₃)₃), 86.83 (COOC(CH₃)₃), 88.29 (C₅H₄, Ci), 146.54 (COOC(CH₃)₃), 148.14 (COOC(CH₃)₃), 149.36 (CO), 169.30 (CO).

Preparation of 1-(*tert*-butoxycarbonyl)-5-ferrocenyl-5-methylimidazolidine-2,4-dione (3). A methanol solution of sodium methoxide (55 μL , 25% in pentane, 0.24 mmol) was added at 0 °C and under argon atmosphere to a solution of **2** (40 mg, 0.08 mmol) in dry methanol (2 mL). After 30 min, the reaction mixture was warmed to 25 °C, stirred for 24 h, then was poured in 5 mL of water and finally the organic layer was separated. The water layer was extracted in ethylacetate (15 mL). The combined organic layers were dried over anhydrous Na₂SO₄, and after filtration the solvent was removed under vacuum to yield a yellow product (30 mg, 94%). Anal. Calcd for $\text{C}_{19}\text{H}_{22}\text{FeN}_2\text{O}_4$: C, 57.30; H, 5.57. Found: C, 57.32; H, 5.58. HRMS (ESI+): m/z Calcd for $\text{C}_{19}\text{H}_{22}\text{FeN}_2\text{O}_4$ (M+): 398.0929. Found: 398.1037. ^1H NMR (acetone-*d*₆): δ 1.47 (s, 9H, COOC(CH₃)₃), 1.90 (s, 3H, CH₃) 4.11 (m, 1H, C₅H₄), 4.17 (s, 5H, C₅H₅), 4.19 (m, 1H, C₅H₄), 4.23 (m, 1H, C₅H₄), 4.40 (m, 1H, C₅H₄), 10.24 (s, 1H, NH). ^{13}C NMR (acetone-*d*₆): δ 24.09 (CH₃), 28.25 (COOC(CH₃)₃), 67.01 (C₅H₄), 67.16 (C5), 68.39 (C₅H₄), 68.49 (C₅H₄), 68.62 (C₅H₄), 70.20 (C₅H₅), 83.58 (COOC(CH₃)₃), 88.76 (C₅H₄, Ci), 149.71 (COOC(CH₃)₃), 152.19 (CO), 173.49 (CO).

X-Ray diffraction. Crystals of **1** and **2** were grown by slow evaporation from methanol and ethyl acetate – *n*-pentane solutions, respectively. X-Ray diffraction data were collected with a Gemini E four-circle kappa diffractometer (Agilent Technologies) equipped with a 92 mm EOS CCD detector, using graphite monochromated Mo K α radiation ($\lambda = 0.71073\text{ \AA}$). Data collection and reduction were performed with the CrysAlisPro software (Agilent Technologies). A semi-empirical absorption correction based on the multi-scan technique using spherical harmonics, implemented in the SCALE3 ABSPACK scaling algorithm, was applied. The structures were solved by *ab initio* procedures of the SIR 2014 program.²⁹ Whereas the structure of **1** belongs to a centrosymmetric space group, namely *Pbca*, as expected for a racemic compound, the structure of **2** could be solved only in the acentric P2₁2₁2₁ space group. Refinement was carried by full-matrix least-squares on F², using all data, by application of the SHELXL-2014 program,³⁰ with anisotropic displacement parameters for all of the non-H atoms. In both structures, the distal Cp ring showed rotational disorder and was refined on two sets of positions, with population parameters of 0.54(3) and 0.46(3) for **1**, while of 0.66(3) and 0.34(3) for **2**. These Cp rings were constrained to the idealized geometry. Restraints were applied to the anisotropic displacement parameters of the carbon atoms of the disordered Cp rings to approach isotropic behaviour. H-Atoms were calculated at idealized positions and refined using a riding model. Initial refinement of the structure of **2** yielded an absolute structure parameter close to 0.5, which indicated the occurrence of an inversion twin. For the final refinement, the TWIN / BASF instructions were included in the instruction file, and the fraction of the second twin domain refined

to 0.48(2). Relevant crystal data and structure refinement parameters for **1** and **2** are listed in Tables S1 and S2 (Supporting Information). CCDC 1531458 and 1531459 contain the supplementary crystallographic data for this paper. The data can be obtained free of charge from The Cambridge Crystallographic Data Centre via www.ccdc.cam.ac.uk/structures.

ASSOCIATED CONTENT

Supporting Information

Crystal data and structure refinement for **1** and **2**. NMR and ESI spectra of **1–3**. CVs of **3** at different concentrations and scan rates. This material is available free of charge via the Internet at <http://pubs.acs.org>.

AUTHOR INFORMATION

Corresponding Author

*Email: saverio.santi@unipd.it

ORCID

Saverio Santi: 0000-0002-6403-4467

Notes

The authors declare no competing financial interest.

ACKNOWLEDGMENT

Financial supports by Italian MIUR (ex-60% grants) and the University of Padova (CPDA142751/14) are acknowledged. We wish to gratefully acknowledge Dr. Renato Schiesari for FT-IR analysis, Dr. Barbara Biondi for ESI-MS analyses and Prof. Alessandro Dolmella (Department of Pharmaceutical Sciences, University of Padova) for granting access to the Gemini diffractometer and for his help with X-ray data collection and processing.

REFERENCES

- (1) Monteiro, J. L.; Piebera, B.; Corrêab, A. G.; Kappe, C. O. *Synlett* **2016**, *27*, 83–87.
- (2) (a) Meusel, M.; Gütschow, M. *Org. Prep. Proced. Int.* **2004**, *36*, 391–443. (b) Gao, W.; Dalton, J. T. *Drug. Discovery Today* **2007**, *12*, 241–248. (c) Cachet, N.; Genta-Jouve, G.; Regalado, E. L.; Mokrini, R.; Amade, P.; Culioli, G.; Thomas, O.P. *J. Nat. Prod.* **2009**, *72*, 1612–1619. (d) Gomes, N. G. M.; Dasari, R.; Chandra, S.; Kiss R.; Kornienko, A. *Mar. Drugs* **2016**, *14*, 98–137. (e) Liu, H.; Yang, Z.; Pan, Z. *Org. Lett.* **2014**, *16*, 5902–5905. (f) Hussain, A.; Kashif, M. K.; Naseer M. M.; Rana, U. A.; Hameed, S. *Res Chem Intermed* **2015**, *41*, 7313–7326. (g) Grewal, A. S.; Bhardwaj, S.; Pandita, D.; Lather, V.; Sekhon, B. S. *Mini Rev. Med. Chem.* **2016**, *16*, 120–162. (h) Chambers, R. K.; Khan, T. A.; Olsen, D. B.; Sleebs, B. E. *Org. Biomol. Chem.* **2016**, *14*, 4970–4985. (i) Marton, J.; Enisz, J.; Hosztafi, S.; Timar, T. *J. Agric. Food Chem.* **1993**, *41*, 148–152. (j) Fan, X.; Jiang, Q.; Sun, Z.; Li, G.; Ren, X.; Liang, J.; Huang, T. S. *Fibers Polym.* **2015**, *16*, 1751–1758.
- (3) (a) Burton, S. G.; Dorrington, R. A.; *Tetrahedron: Asymmetry* **2004**, *15*, 2737–2741. (b) Fernández-Nieto, F.; Mas Roselló, J.; Lenoir, S.; Hardy, S. *Org. Lett.* **2015**, *17*, 3838–3841. (c) Ware, E.; *Chem. Rev.* **1950**, *46*, 403–470. (d) López, C. A.; Trigo, G. G. *Adv. Heterocycl. Chem.* **1985**, *38*, 177–228. (e) Murray, R. G.; Whitehead, D. M.; Le Strat, F.; Conway, S. *Org. Biomol. Chem.* **2008**, *6*, 988–991.
- (4) (a) Chattopadhyay, B.; Mukherjee, A. K.; Narendra, N.; Hemantha, H. P.; Sureshbabu, V. V.; Helliwell, M.; Mukherjee, M. *Cryst. Growth Des.* **2010**, *10*, 4476–4484. (b) Delgado, G. E.; Rodríguez, J. A.; Mora, A. J.; Bruno-Colmenárez, J.; Uzcátegui, J.; Chacón, C. *Mol. Cryst. Liq. Cryst.* **2016**, *629*, 96–104.
- (5) (a) Payen, O.; Top, S.; Vessières, A.; Brulé, E.; Plamont, M.-A.; McGlinchey, M. J.; Müller-Bunz, H.; Jaouen, G. *J. Med. Chem.* **2008**, *51*, 1791–1799. (b) Top, S.; Thibaudeau, C.; Vessières, A.; Brule, E.; Le Bideau, F.; Joerger, J.-M.; Plamont, M.-A.; Samreth, S.; Edgar, A.; Marrot, J.; Herson, P.; Jaouen, G. *Organometallics* **2009**, *28*, 1414–1424.
- (6) Braga, S. S.; Silva, A. M. S.; *Organometallics* **2013**, *32*, 5626–5639.
- (7) Navarro, M.; Castro, W.; Biot, C.; *Organometallics* **2012**, *31*, 5715–5727.
- (8) (a) Weiss, J. *Coord. Chem. Rev.* **2010**, *254*, 2247–2248. (b) *Nano and Molecular Electronics handbook*, Lyshevski, S. E., Ed.; CRC Press, New York, 2007. (c) Bayley, H. *Nature* **2010**, *467*, 164–165. (d) Giacalone, F.; Martin, N. *Adv. Mater.* **2010**, *22*, 4220–4248. (e) Jurow, M.; Schuckman, A. E.; Batteas, J. D.; Drain, C. M. *Coord. Chem. Rev.* **2010**, *254*, 2297–2310. (f) Chung, A.; Deen, J.; Lee, J.-S.; Meyyappan, V. *Nanotechnology* **2010**, *21*, 412001. (g) Balzani, V.; Credi, V.; Venturi, V. *Nano Today* **2007**, *2*, 18–25. (h) Santi, S.; Bisello, A.; Cardena, R.; Donoli, A. *Dalton Trans* **2015**, *44*, 5234–5257. (i) *Ferrocenes: Ligands, Materials and Biomolecules*; Štěpnička, P., Ed.; Wiley: Chichester, England, 2008. (j) Moriuchi, T.; Hirao, T. *Chem. Soc. Rev.* **2004**, *33*, 294–301. (k) Severin, K.; Bergs, R.; Beck, W. *Angew. Chem. Int. Ed.* **1998**, *37*, 1634–1654. (l) Paleček, E.; Tkáč, J.; Bartošík, M.; Bertók, T.; Ostatná, V.; Paleček, J. *Chem. Rev.* **2015**, *115*, 2045–2108. (m) Sun, R. L.; Wang, L.; Yu, H. J.; Abdin, Z. U.; Chen, Y. S.; Huang, J.; Tong, R. B. *Organometallics* **2014**, *33*, 4560–4573.
- (9) (a) De Cola, L.; Belsler, P. Photonic Wires Containing Metal Complexes, In *Electron Transfer in Chemistry*; Balzani, V., Ed.; Wiley-VCH: Weinheim, Germany, 2001; vol. 5, pp. 97–136. (b) Paddock-Row, M. N. Covalently Linked Systems Based on Organic Components, In *Electron Transfer in Chemistry*; Balzani, V., Ed.; Wiley-VCH, Weinheim, Germany, 2001; vol. 2, pp. 179–271. (c) Joachim, C.; Gimzewski, J. K.; Aviram, A. *Nature* **2000**, *408*, 541–548.
- (10) Chaubey, A.; Malhotra, B. D. *Biosens. Bioelectron.* **2002**, *17*, 441–456.
- (11) Molina, P.; Tárraga, A.; Caballero, A. *Eur. J. Inorg. Chem.* **2008**, *2008*, 3401–3417.
- (12) Fehér, C.; Papp, M.; Gömöry, Á.; Nagy, Wouters, J.; Lendvay, G.; Skoda-Földes, R. *Organometallics* **2016**, *35*, 4023–4032.
- (13) (a) Lapić, J.; Pavlović, G.; Siebler, D.; Heinze, K.; Rapić, V. *Organometallics* **2008**, *27*, 1447–1453. (b) Siebler, D.; Förster, C.; Gasi, T.; Heinze, K. O. *Organometallics* **2011**, *30*, 313–327. (c) Adhikari, B.; Afrasiabi, R.; Kraatz, H.-B. *Organometallics* **2013**, *32*, 5899–5905. (d) Adhikari, B.; Lough, A. J.; Barker, B.; Shah, A.; Xiang, C.; Kraatz H.-B. *Organometallics* **2014**, *33*, 4873–4887. (e) Jinrui Deng, D.; Biao Zhao, B.; Deng J.; *Ind. Eng. Chem. Res.* **2016**, *55*, 7328–7337.
- (14) (a) Lapić, J.; Pavlović, G.; Siebler, D.; Heinze, K.; Rapić, V. *Organometallics* **2008**, *27*, 726–735. (b) Tebben, L.; Bussmann, K.; Hegemann, M.; Kehr, G.; Fröhlich, R.; Erker, G. O. *Organometallics* **2008**, *27*, 4269–4272. (c) Köster, S. D.; Dittrich, J.; Gasser, G.; Hüsken, N.; Henao-Castañeda, I. C.; Jios, J. L.; Della Vedova, C. O.; Metzler-Nolte, N. *Organometallics* **2008**, *27*, 6326–6332. (d) Gasser, G.; Belousoff, M. J.; Bond, A. M.; Spiccia, L. J. *Org. Chem.* **2006**, *71*, 7565–7573. (e) Donoli, A.; Marcuzzo, V.; Moretto, A.; Crisma, M.; Toniolo, C.; Cardena, R.; Bisello, A.; Santi, S. *Org. Lett.* **2011**, *13*, 1282–1285. (f) Donoli, A.; Marcuzzo, V.; Moretto, A.; Crisma, M.; Toniolo, C.; Cardena, R.; Bisello, A.; Santi, S. *Biopolymers* **2013**, *100*, 14–24.
- (15) (a) Moriuchi, T.; Nomoto, A.; Yoshida, K.; Ogawa, A.; Hirao, T. *J. Am. Chem. Soc.* **2001**, *123*, 68–75. (b) Moriuchi, T.; Yoshida, K.; Hirao, T. *Org. Lett.* **2003**, *5*, 4285–4288. (c) Kraatz, H.-B.; Bediako-Amoa, I.; Gyepi-Garbrah, S. H.; Sutherland T. C. *J. Phys. Chem. B* **2004**, *108*, 20164–20172. (d) Baršič, L.; Čakić, M.; Mahmoud, K. A.; Liu, Y.; Kraatz, H.-B.; Pritzkow, H.; Kirin, S. I.; Metzler-Nolte, N.; Rapić, V. *Chem.-Eur. J.* **2006**, *12*, 4965–4980. (e) Moriuchi, T.; Nagai, T.; Hirao, T. *Org. Lett.* **2006**, *8*, 31–34; (f) Kirin, S. I.; Kraatz, H.-B.; Metzler-Nolte, N. *Chem. Soc. Rev.* **2006**, *35*, 348–356. (g) Lataifeh, A.; Beheshti, S.; Kraatz, H.-B. *Eur. J. Inorg. Chem.* **2009**, *2009*, 3205–3218. (h) Moriuchi, T.; Hirao, T. *Acc. Chem. Res.* **2010**, *43*, 1040–1051. (i) Amdursky, N. *ChemPlusChem* **2015**, *80*, 1075–1095. (j) Shah, A.; Adhikari, B.; Martić, S.; Munir, V.; Shahzad, S.; Ahmade, K.; Kraatz H.-B. *Chem. Soc. Rev.* **2015**, *44*, 1015–1027.
- (16) (a) Kraatz, H.-B.; Bediako-Amoa, I.; Gyepi-Garbrah, S. H.; Sutherland, T. C. *J. Phys. Chem. B* **2004**, *108*, 20164–20172. (b) Sek,

- S.; Tolak, A.; Misicka, A.; Palys, B.; Bilewicz, R. *J. Phys. Chem. B* **2005**, *109*, 18433–18438. (c) Morita, T.; Kimura, S. *J. Am. Chem. Soc.* **2003**, *125*, 8732–8733. (d) Takeda, K.; Morita, T.; Kimura, S. *J. Phys. Chem. B* **2008**, *112*, 12840–12850. (e) Okamoto, S.; Morita, T.; Kimura, S. *Langmuir* **2009**, *25*, 3297–3304. (f) Arikuma, Y.; Takeda, K.; Morita, T.; Ohmae, M.; Kimura, S. *J. Phys. Chem. B* **2009**, *113*, 6256–6266. (g) Brooksby, P. A.; Anderson, K. H.; Downard, A. J.; Abell, A. D. *Langmuir* **2010**, *26*, 1334–1339. (h) Arikuma, Y.; Nakayama, H.; Morita, T.; Kimura, S. *Angew. Chem., Int. Ed.* **2010**, *49*, 1800–1804. (i) Arikuma, Y.; Nakayama, H.; Morita, T.; Kimura, S. *Langmuir* **2011**, *27*, 1530–1535. (j) Brooksby, P. A.; Anderson, K. H.; Downard, A. J.; Abell, A. D. *J. Phys. Chem. C* **2011**, *115*, 7516–7526. (k) Mandal, H. S.; Kraatz, H.–B. *J. Phys. Chem. Lett.* **2012**, *3*, 709–713. (l) Lima, F. C. D. A.; Calzolari, A.; Caldas, M. J.; Iost, R. M.; Crespilho, F. N.; Pettrilli, H. M. *J. Phys. Chem. C* **2014**, *118*, 23111–23116.
- (17) (a) Pichlmaier, M.; Winter, R. F.; Zabel, M.; Zalis, S. *J. Am. Chem. Soc.* **2009**, *131*, 4892–4903. (b) Sun, H.; Steeb, J.; Käfer, A. E. *J. Am. Chem. Soc.* **2006**, *128*, 2820–2821. (c) Tadokoro, M.; Inoue, T.; Tamaki, S.; Fujii, K.; Isogai, K.; Nakazawa, H.; Takeda, S.; Isobe, K.; Koga, N.; Ichimura, A.; Nakasuji, K. *Angew. Chem., Int. Ed.* **2007**, *46*, 5938–5942. (d) Goeltz, J. C.; Kubiak, C. P. *J. Am. Chem. Soc.* **2010**, *132*, 17390–17392. (e) Wilkinson, L. A.; McNeill, L.; Meijer, A. J. H. M.; Patmore, N. *J. Am. Chem. Soc.* **2013**, *135*, 1723–1726.
- (18) Bucherer, H. T.; Lieb, V. A. *J. Prakt. Chem.* **1934**, *141*, 5–43.
- (19) Fu, Y.; Zhou, Z.; Hazendonk, P.; Bain, A. D.; Fronczek, F. R.; Escobedo, J.; McLaughlin, M. L.; Hammer, R. P. *J. Mol. Struct.* **2004**, *687*, 65–72.
- (20) Nadvorný, D.; Da Silva, J. B. P., *Int. J. Quantum Chem.* **2011**, *111*, 1436–1443.
- (21) (a) Groom, C. R.; Bruno, I. J.; Lightfoot, M. P.; Ward, S. C. *Acta Crystallogr.* **2016**, *B72*, 171–179. (b) Florencio, F.; Smith–Verdier, P.; García–Blanco, S. *Acta Crystallogr.* **1978**, *B34*, 2220–2223. (c) Wermuth, U. D.; Jenkins, I. D.; Bott, R. C.; Byriel, K. A.; Smith, G. *Aust. J. Chem.* **2004**, *57*, 461–465. (d) Eitel, S. H.; Jautze, S.; Frey, W.; Peters, R. *Chem. Sci.* **2013**, *4*, 2218–2233. (e) Kashif, M. K.; Hussain, A.; Rauf, M. K.; Ebihara, M.; Hameed, S. *Acta Crystallogr.* **2008**, *E64*, o444. (f) Stalker, R. A.; Munsch, T. E.; Tran, J. D.; Nie, X.; Warmuth, R.; Beatty, A.; Aakeroy, C. B. *Tetrahedron* **2002**, *58*, 4837–4849. (g) Koos, M.; Steiner, B.; Langer, V.; Gyepesova, D.; Durik, M. *Carbohydr. Res.* **2000**, *328*, 115–126. (h) Graus, S.; Uriel, S.; Serrano, J. L. *CrystEngComm* **2012**, *14*, 3759–3766.
- (22) Sbarbati Nudelman, N.; Alvaro C. E. S. *J. Phys. Org. Chem.* **2011**, *24* 1067–1071.
- (23) Pysh, E. S.; Toniolo, C. *J. Am. Chem. Soc.* **1977**, *99*, 6211–6219.
- (24) Baruah, P. K.; Gonnade, R.; Phalgune, U. D.; Sanjayan, G. *J. Org. Chem.* **2005**, *70*, 6461–6467.
- (25) Isse, A. A.; Gennaro, A.; Vianello, E. *Electrochim. Acta*, **1992**, *37*, 113–118.
- (26) Bard, A. J.; Faulkner, R. *Electrochemical Methods*, Wiley, New York, 2001; p. 231.
- (27) (a) Bax, A.; Subramanian, S. *J. Magn. Reson.* **1986**, *67*, 565–569. (b) Parella, T. *Magn. Reson. Chem.* **1998**, *36*, 467–495. (c) Ruiz-Cabello, J.; Vuister, G. W.; Moonen, C. T. W.; van Gelderen, P.; Cohen, J. S.; van Zijl, P. *J. Magn. Reson.* **1992**, *100*, 282–302. (d) Willker, W.; Leibfritz, D.; Kerrsebaum, R.; Bermel, W. *Magn. Reson. Chem.* **1993**, *31*, 287–292. (e) Bax, A.; Summers, M. F. *J. Am. Chem. Soc.* **1986**, *108*, 2093–2094. (f) Summers, M. F.; Marzilli, L. G.; Bax, A. *J. Am. Chem. Soc.* **1986**, *108*, 4285–4294.
- (28) Amatore, C.; Lefrou, C.; Pflüger, F. *J. Electroanal. Chem.* **1989**, *270*, 43–59.
- (29) Burla, M. C.; Caliandro, R.; Carrozzini, B.; Cascarano, G.L.; Cuocci, C.; Giacobozzo, C.; Mallamo, M.; Mazzone, A.; Polidori, G. *J. Appl. Crystallogr.* **2015**, *48*, 306–309.
- (30) Sheldrick, G. M. *Acta Crystallogr. C* **2015**, *71*, 3–8.

The synthesis of the ferrocenyl methylhydantoin (5-ferrocenyl-5-methylimidazolidine-2,4-dione) and its derivatives with the protecting group *tert*-butoxycarbonyl (Boc), 1,3-di(*tert*-butoxycarbonyl)-5-ferrocenyl-5-methylimidazolidine-2,4-dione, and 1-(*tert*-butoxycarbonyl)-5-ferrocenyl-5-methylimidazolidine-2,4-dione allowed an in depth multitechnique (X-Ray, NMR, FT-IR, ESI-MS, Cyclic and Differential Pulse Voltammetry) investigation on how C=O···H–N hydrogen bonds can induce hydantoin dimerization.

